CHICAGO JOURNALS

The Ultraviolet Spectrum of VV Cephei Out of Eclipse
Author(s): Wendy Hagen Bauer and Philip D. Bennett
Source: *Publications of the Astronomical Society of the Pacific*, Vol. 112, No. 767 (January 2000), pp. 31-49
Published by: The University of Chicago Press on behalf of the Astronomical Society of the Pacific
Stable URL: http://www.jstor.org/stable/10.1086/316479
Accessed: 10/10/2011 08:22

Your use of the JSTOR archive indicates your acceptance of the Terms & Conditions of Use, available at
http://www.jstor.org/page/info/about/policies/terms.jsp

JSTOR is a not-for-profit service that helps scholars, researchers, and students discover, use, and build upon a wide range of content in a trusted digital archive. We use information technology and tools to increase productivity and facilitate new forms of scholarship. For more information about JSTOR, please contact support@jstor.org.

The University of Chicago Press and *Astronomical Society of the Pacific* are collaborating with JSTOR to digitize, preserve and extend access to *Publications of the Astronomical Society of the Pacific.*

http://www.jstor.org

PUBLICATIONS OF THE ASTRONOMICAL SOCIETY OF THE PACIFIC, 112:31–49, 2000 January
© 2000. The Astronomical Society of the Pacific. All rights reserved. Printed in U.S.A.

The Ultraviolet Spectrum of VV Cephei Out of Eclipse

WENDY HAGEN BAUER

Whitin Observatory, Wellesley College, Wellesley, MA 02481; wbauer@wellesley.edu

AND

PHILIP D. BENNETT

Center for Astrophysics and Space Astronomy, University of Colorado, Campus Box 389, Boulder, CO 80309-0389; pbennett@casa.colorado.edu

Received 1998 October 6; accepted 1999 September 15

ABSTRACT. The *International Ultraviolet Explorer* (*IUE*) satellite observed VV Cephei (M2 Iab+B?) over nearly a full 20.3 year orbital period, but all the observations were obtained outside total eclipse. Egress of the chromospheric eclipse was the only portion of the eclipse observed by *IUE*. We have examined all 124 high-resolution *IUE* spectra of VV Cephei and describe the spectrum and its variations.

Contrary to initial expectations, the spectrum remained complex throughout the entire orbit, and five line components have been identified: (1) emission lines; (2) neutral, low-excitation (e.g., Fe I) lines, which disappear as the hot component emerges from eclipse; (3) broad, high-ionization (e.g., Si IV and Fe III) lines arising from the hot component or nearby circumstellar material; (4) narrow absorption cores from the circumstellar envelope of the M supergiant; and (5) "shell" absorption lines with variable profiles which do not absorb below a minimum depth.

Mg II *h* and *k* emission broadens and strengthens when the system is near periastron and secondary eclipse. Most of the variation in the other emission features appears to be stochastic rather than phase dependent.

The continuum shows rapid variations on timescales as short as 2 weeks. At any one time, the continuum flux between 1400 and 3000 Å is fairly constant but varies, apparently stochastically, in the range $(2–7) \times 10^{-12}$ ergs s^{-1} cm^{-2} Å^{-1} for observations obtained outside of chromospheric eclipse. The dereddened continuum fluxes vary as $\sim\lambda^{-0.8}$, implying that the source is not purely stellar.

Radial velocity measurements of the circumstellar and shell lines show that neither follows the radial velocity curve of the two stars. Circumstellar line velocities range from the systemic velocity to $\sim$15 km s^{-1} more negative, consistent with their formation in an extended circumstellar envelope of the M supergiant which is large compared to the scale of the orbit. The shell lines are redshifted from the systemic velocity by $\sim$30 km s^{-1}. The last *IUE* observations (near phase 0.9) showed shell lines with greater redshifts and deeper absorption than around the rest of the cycle.

The ultraviolet spectrum of VV Cep is compared to spectra of stars showing similar features: the Be shell star 28 Tauri, the B[e] star HD 45677, and the M supergiant + B binary systems α Scorpii and KQ Puppis. A table detailing the appearance and behavior of numerous line multiplets is presented.

1. INTRODUCTION

VV Cephei is an eclipsing binary consisting of an M2 Iab supergiant and a smaller, hotter companion, with a 20.3 year period. Orbital elements have been determined by Wright (1977), who used Hα observations over an entire period to map out a stream of material flowing from the M supergiant and apparently accreting onto the hot companion. It is not clear whether the M supergiant fills its Roche lobe at periastron. With a mass ratio of unity and a minimum separation of 2.5×10^9 km, the Roche lobe radius would be half the separation, or 1800 $R_\odot$. Determinations of the M-star radius from the past two eclipses range from below to above this value: 1600 (Wright 1977), 1700 (Nakagiri & Yamashita 1979), 1850 (Mollenhoff & Schaifers 1981), and 1900 $R_\odot$ (Saito 1980). The orbit as determined by Wright (1977) is shown in Figure 1.

VV Cep is similar to the ζ Aurigae stars, in which a B-type main-sequence star is eclipsed by a K supergiant. As the B star shines through the extended atmosphere of the supergiant, its orbital motion can be used as a probe with which to study the spatial structure of the supergiant's atmosphere. Such work is best done in the ultraviolet region of the spectrum, where the cool supergiant's contribution to the observed continuum is negligible. Observing in the

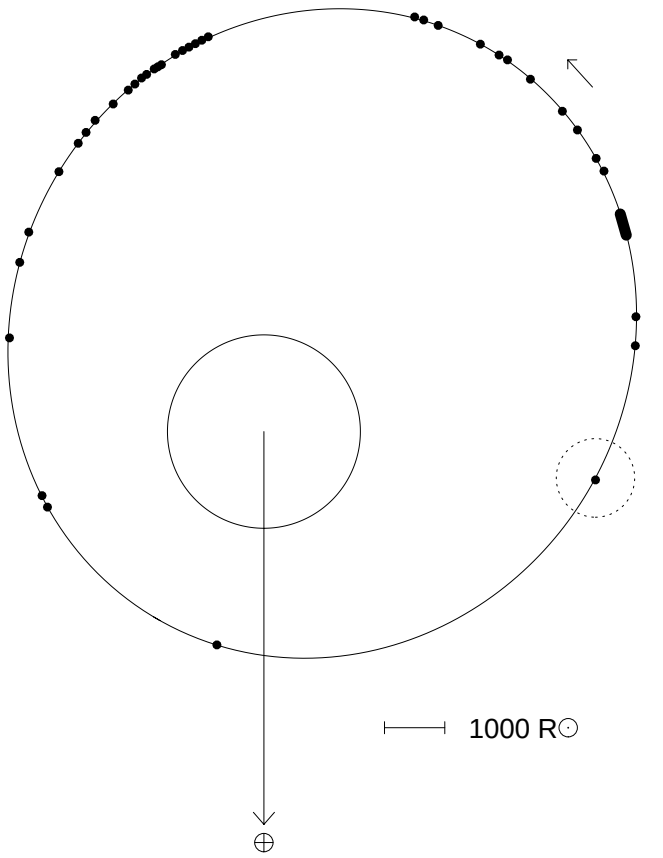

FIG. 1.—The orbit of VV Cep to scale, as determined by Wright (1977). The large circle in the center is the M supergiant. Small filled circles represent the positions of the hot component in its orbit at the times *IUE* observations were made. The dotted circle represents the size of the disk around the hot component, as determined (near apastron) by Wright (1977).

ultraviolet also allows us to study the nature of the hot component itself. In this paper, we restrict the discussion to an analysis of the ultraviolet spectrum observed by the *International Ultraviolet Explorer* (*IUE*) satellite. For other aspects of VV Cep and similar binaries, the reader is directed to the following: Cowley (1969) for a general review of VV Cephei stars, Wright (1970) for a review of ζ Aur stars including VV Cep, Wright (1977) for an analysis of the orbit as derived from the behavior of the Hα line, van de Kamp (1977) for the astrometric orbit, Guinan et al. (1986) for photometric variability, and Hjellming (1985) for the radio properties.

At the resolution of the *IUE* satellite, the UV spectra of the ζ Aurigae systems far from eclipse are similar to those of normal B stars. However, when the UV spectrum of VV Cep was observed during egress from eclipse in 1978, the spectrum remained complex well outside eclipse (Hagen et al. 1980), and the continuum is variable and probably not stellar. The true nature of the hot component remains uncertain. The origin of the UV continuum remain unclear; however, it cannot be purely stellar because of the observed variability of at least a factor of 2. Its mass is 20 $M_{\odot}$ (Wright 1977), corresponding to a normal main-sequence star of spectral type O9 (Schmidt-Kaler 1982). Strong absorption lines of Si IV indicate a spectral type of about B1 or B2 (Bauer, Stencel, & Neff 1991). Hack, Engin, & Yilmaz (1989) fit the falloff in the UV flux at wavelengths shorter than 1400 Å as due to continuum turnover and determined a spectral type of A0 II. However, this turnover is consistent with interstellar and/or circumstellar absorption from the damping wings of Lyα superposed on an early B-type spectrum.

The *IUE* satellite observed VV Cep over nearly an entire orbital period, from egress from eclipse in 1978–1995. The observations made through early 1990 were described by Bauer et al. (1991). Even out of eclipse, the hot component remained shrouded in a rich line spectrum, similar to that of the ζ Aurigae binary 31 Cygni as seen during chromospheric eclipse. Significant variations in these line profiles were observed on timescales as short as 2 weeks, leading Stencel, Potter, & Bauer (1993) to observe the system every 2 weeks from 1991 July through October. Variations as large as a factor of 2 in the integrated flux from 1000 to 2000 Å were seen over a 2 week interval, with parallel, though smaller, variation in the 2000–3000 Å region.

In this paper, we present a summary of the extensive *IUE* data and attempt to classify spectral line formation in the ultraviolet spectrum. This spectrum is complex and contains contributions from several physically distinct line-forming regions, and it is not yet certain where these regions are located in the binary system. It is the goal of this paper to categorize the line-forming regions observed by *IUE* in order to further the construction of physical models of this complex binary.

A representative section of the *IUE* out-of-eclipse spectrum of VV Cep is plotted in Figure 2. Study of these complex spectra has revealed five distinct line components. In most regions of the UV spectrum of VV Cep, there is a recognizable continuum, upon which the following components are superimposed:

1. *Emission lines*, most of which are due to Fe II.
2. *Broad absorption lines* attributed to the photosphere of the hot component, or hot circumstellar gas, possibly accreting onto the hot star (see Fig. 2 in Bauer et al. 1991). These lines include Si IV (1), Fe III (34), Al III (1), and C IV (1).
3. *Neutral absorption lines* which weaken and disappear during egress (see Fig. 5 in Bauer et al. 1991). Although not all these lines are yet identified, those that have been identified all arise from neutral elements.
4. *Shell absorption lines*, so called because this rich absorption spectrum more closely resembles the Be star 28 Tauri during a strong shell phase than the chromospheric

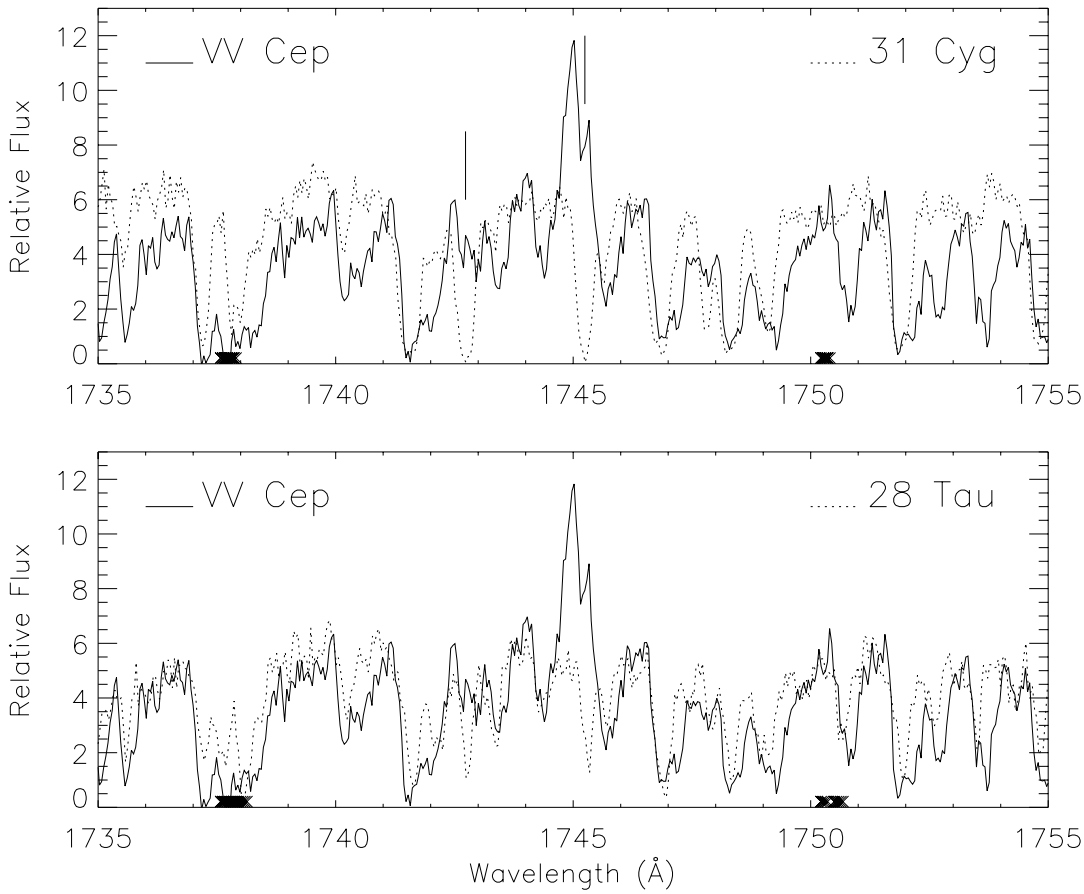

FIG. 2.—A comparison of a representative region of the spectra of VV Cep, 31 Cyg, and 28 Tau. Solid vertical lines mark the wavelengths of N I (9). The VV Cep observation is SWP 38281, obtained 1990 March 1 ($\phi = 0.617$), near third quadrature. 31 Cyg (SWP 17845) was observed in chromospheric eclipse, on 1982 September 3, and 28 Tau (SWP 5986) was observed during strong shell phase on 1979 July 29. Fluxes for VV Cep are in units of 10^{-12} ergs s^{-1} cm^{-2} Å^{-1}. Relative flux of 13 corresponds to 2.0×10^{-10} ergs s^{-1} cm^{-2} Å^{-1} for both 31 Cyg and 28 Tau.

eclipse phase of 31 Cyg. Most of these lines arise from singly ionized iron-group elements. The profiles of these "shell" lines can vary significantly over timescales as short as 2 weeks, indicating that at least some of this absorption occurs over a small volume, presumably in material being accreted by the hot component. The line profiles can be symmetric, or can show additional red- or blueshifted absorption (see Fig. 11 in Bauer et al. 1991). There is a minimum depth, or "pedestal," below which the shell lines do not absorb.

5. *Circumstellar absorption lines* which are narrower than the typical shell lines. Some of these are associated with emission lines, and some have greater central depth than the shell lines. They do not share the line profile variations of the shell spectrum. These components are likely due to the extended circumstellar envelope of the M-supergiant primary.

In order to gain more insight into the complex ultraviolet spectrum of VV Cep, we have compared it to several objects which show related spectra. Two B stars are good analogs for portions of the UV spectrum of VV Cep. Nearly all of VV Cep's absorption features are seen in the strong shell spectrum of 28 Tau. Nearly all the emission features in VV Cep are seen in the UV spectrum of the B[e] star HD 45677; furthermore, like HD 45677, VV Cep shows forbidden lines in its optical spectrum (Kawabata & Saito 1997). The visual binary α Sco, whose components are similar to but far more widely separated than those of VV Cep, shows some of the same absorption and emission features, but more weakly. However, all the out-of-eclipse components of the VV Cep spectrum are shown by the binary system KQ Puppis (M1–2 Iab + B) when it is near periastron.

This paper is organized as follows: § 2 discusses the *IUE* observations. Because the UV spectrum of VV Cep is so dominated by lines, the low-resolution *IUE* spectra provide essentially no information about the continuum. Line-free regions were found in the high-dispersion spectra. The shape of and variations in this continuum and in the

minimum depth of the shell lines are discussed in § 3. We then present a table detailing the appearance and behavior of prominent multiplets in VV Cep and related objects. The absorption-line spectrum is discussed in § 4 and the emission lines in § 5. In § 6, we compare the spectrum of VV Cep to the related objects listed above, with a summary in § 7.

2. OBSERVATIONS

The *IUE* satellite began observing VV Cep during its initial commissioning period, late in the partial phase of egress from eclipse in 1978. Although the expected lifetime of the satellite was only 5 years, the last exposure of VV Cep was made more than 17 years later, in 1995 November. After this, the aging satellite could no longer observe the system because of the lack of a suitable guide star. Nearly a full orbital cycle was observed, but neither ingress into eclipse nor totality was observed.

Table 1 lists all high-resolution *IUE* spectra taken of VV Cep in the 1990s. A similar listing can be found for earlier observations in Bauer et al. (1991); although all observation dates with usable images are listed in that reference, not all individual images obtained on a given date were listed. All of the observations listed in Table 1 were made through the large aperture.

Phases (ϕ) were calculated from mid–primary eclipse, using a period of 7430.5 days (Wright 1977) and epoch of

TABLE 1

HIGH-RESOLUTION *IUE* OBSERVATIONS OF VV CEPHEI (1990–1995)

Date (UT)	JD (+2,400,000)	Phase	LWP Image	Exposure Time (minutes)	SWP Image	Exposure Time (minutes)
1990 Mar 1	47,952	0.6174	17446	30	38281	90
1990 Jun 22.....	48,065	0.6326	...	...	39135	140
1991 Jun 6	48,414	0.6795	20533	30	41782	90
1991 Jun 20.....	48,428	0.6814	20648	25	41886	90
1991 Jul 6	48,444	0.6835	20755	20	42013	90
1991 Jul 21.....	48,459	0.6855	20858	20	42109	90
1991 Aug 5.....	48,474	0.6876	20957	20	42176	90
1991 Aug 19	48,488	0.6895	21041	20	42289	90
1991 Sep 3	48,503	0.6915	21143	20	42384	90
1991 Sep 19.....	48,519	0.6936	21284	20	42511	90
1991 Sep 30.....	48,530	0.6951	21371	20	42585	90
		0.6951	...	...	42587	90
1991 Oct 15.....	48,545	0.6971	21496	20	42727	90
1991 Oct 30.....	48,560	0.6991	21569	20	42942	90
1992 Jun 5	48,779	0.7286	23254	20	44867	90
		0.7287	23256	20	44870	90
		0.7287	23257	14	...	...
1992 Aug 7.....	48,842	0.7371	23660	20	45301	90
1992 Oct 2	48,898	0.7446	24049[a]	16	...	...
1993 Jan 2	48,990	0.7570	...	...	46646	60
1993 Jan 15	49,003	0.7588	24736	20	46733	60
1993 Feb 8	49,027	0.7619	24864	25	46899	75
1993 Feb 16	49,035	0.7631	24933	20	46973	90
1993 May 26.....	49,134	0.7764	25605	20	47741	75
1994 Jan 10	49,363	0.8072	27204	20	49802	90
1994 Jan 20	49,373	0.8086	27259	20	49854	90
1994 Jun 15.....	49,519	0.8282	28425	15	51102	240
		0.8282	...	...	51106	85
1994 Jun 16.....	49,520	0.8284	28434	15	51113	90
1994 Jul 7	49,541	0.8312	28567	20	51348	90
1994 Jul 25.....	49,559	0.8336	28730	20	51601	90
		0.8336	28731	20	...	...
1994 Nov 20	49,677	0.8494	29538	15	52839	90
1995 Jun 21	49,890	0.8782	30938	15	55056	90
1995 Sep 10.....	49,971	0.8890	...	...	55899	75
1995 Nov 9	50,031	0.8971	31678	20	56172	90

[a] Unusable because of a high background which causes the entire image to be saturated.

mideclipse of HJD = 2,443,365. This epoch was determined from the mean of second and third contacts from Hα and Hβ observations by Mollenhoff & Schaifers (1981) and photometry by Nakagiri & Yamashita (1979). These values agree well with those determined by Hack et al. (1989), but are 0.002–0.003 less than those calculated by Bauer et al. (1991), who used the epoch of Wright's (1977) *calculated* time of mideclipse, which is 17 days (0.0023 of a period) earlier than the *observed* time of mideclipse he quoted.

Figure 1 shows the orbit of VV Cep and the size of the M supergiant to scale, as determined by Wright (1977). The small filled circles represent the positions of the hot component at the times of the *IUE* observations. The dotted circle represents the size of the accretion disk or envelope surrounding the hot component, as determined from eclipse observations by Wright (1977). The point in the center of the disk represents the observation of 1988 August 25, the last observation of the 1980s. The observation directly above this in Figure 1 is the first one in Table 1. The observations listed in this table were all made between third quadrature and ingress. For several months in 1991, the system was monitored every 2 weeks (see Stencel, Potter, & Bauer 1993 for a discussion of the variations in the low-dispersion observations made over this period). These points overlap to produce what looks like a line along this part of the orbit.

As a result of the convolution of the response of the detector and the continuum, most of the exposures were only useful from 1600 to 1900 Å for SWP exposures and from 2500 to 3000 Å for LWR/LWP images. Only three SWP images were exposed long enough to be useful much below 1600 Å: SWP 3322, obtained during egress from chromospheric eclipse; SWP 13383, obtained shortly before first quadrature; and SWP 51102, obtained after third quadrature. A few LWR/P exposures (mostly made during egress from eclipse) were long enough to provide some useful information below 2500 Å.

Unless otherwise noted, all figures in this paper were prepared using data from the final *IUE* (NEWSIPS) archive, and the units for flux are ergs s^{-1} cm^{-2} $Å^{-1}$. Unreliable data are marked with crosses. Where the crosses are below the spectrum, they are marking reseaux, the fiducial marks on the *IUE* detectors, and where they are above the spectrum, they are generally marking saturated pixels. Any exceptions are described in the individual figure captions. All data for SWP 42942 are from SIPS processing, as that image had not been processed with NEWSIPS at the time of writing. LWR 1525 is not archived as either SIPS or NEWSIPS data.

The final *IUE* archive gives wavelengths as observed in a vacuum. For this paper, wavelengths longer than 2000 Å were converted to air wavelengths.

In all figures (unless specifically noted in the caption), the wavelength scale has been further corrected for the systemic velocity for binaries: -20 km s^{-1} for VV Cep (Wright 1977) and -8 km s^{-1} for 31 Cyg (Wright 1970). The radial velocity of 28 Tau is highly variable; the SIMBAD database lists values from -32 to 23 km s^{-1}. Therefore, no wavelength correction for radial velocity has been applied for 28 Tau.

3. THE CONTINUUM

Hagen et al. (1980) integrated *IUE* low-resolution observations to show the increase of flux as the hot component emerged from eclipse. The high-resolution spectra have so many lines that they dominate the overall flux distribution. Therefore, we have used high-resolution large-aperture spectra to identify line-free regions of the continuum, which range from 0.5 to 6 Å in extent, and have determined the median value of the flux over these intervals. VV Cep has a reddening of $E(B-V) = 0.4$ (Hack et al. 1989), which corresponds to a visual extinction $A_V = 1.2$. In order to examine the intrinsic behavior of the continuum fluxes, we first dereddened the spectrum using the ultraviolet extinction law of Cardelli, Clayton, & Mathis (1989). Observed and dereddened continua for two phases selected for relatively high and low flux are plotted in Figure 3. The continuum flux F_λ varies approximately as $\lambda^{-0.8}$ over the entire wavelength range. The *IUE* continuum is relatively flat, falling off much less steeply than the continuum of a B0 star, which has a $\sim\lambda^{-3}$ dependence in the *IUE* spectral region. This continuum behavior implies that the source is not purely stellar.

Rapid variations have been observed in the hot continuum. Because of the relative flatness of the continuum, we have averaged the continuum fluxes in the SWP and LWP/R regions, omitting wavelengths with inconsistent measurements we believe unlikely to represent a true continuum. Some of the regions were rejected because they were consistently low in most observations, and others (in the LWR/P region) because they were high in observations in which the most clearly line-free regions were low, and are thus likely contaminated by emission (see lower panel of upper half of Fig. 3). These mean values are plotted against phase in Figure 4. The values around phase 0.05 (which are plotted on an expanded scale in the lower left-hand panel of Fig. 4), do show egress from eclipse, but apparently stochastic variations dominate the continuum values observed around the rest of the cycle. The data obtained during the 1991 monitoring period are plotted with an expanded timescale in the lower right-hand panel of Figure 4. Note the large variation between the last two of these observations; they nearly span the full range of continuum fluxes observed outside of eclipse around the entire cycle. These rapid variations, coupled with the flatness of the ultraviolet continuum,

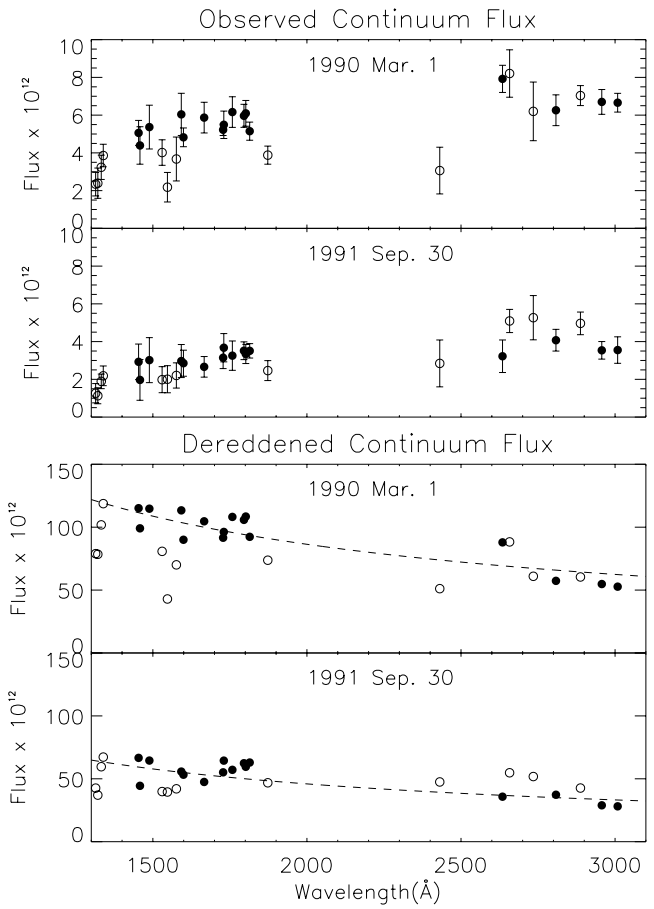

FIG. 3.—The continuum as a function of wavelength in the UV spectrum of VV Cep. The upper two panels plot the observed continuum fluxes, and the lower two panels plot the dereddened fluxes. The circles are plotting the *median* value of the continuum as determined within line-free regions of the spectrum. Error bars represent the standard deviation from the *mean* value. The continua at wavelengths plotted with open circles were not always consistent with those plotted with filled circles and were excluded when the continuum was averaged over the SWP and LWR/P regions. The dashed lines in the lower two panels represent a $\lambda^{-0.8}$ power law fit to the data. The 1990 March 1 data are from LWP 17446 and SWP 38281 ($\phi = 0.617$) and the 1991 September 30 data are from LWP 21372 and SWP 42587 ($\phi = 0.695$).

imply that a substantial fraction of this continuum is not stellar.

In general, if the continuum is high in the LWR/P region, it also tends to be high in the SWP region. For phases at which both LWR/P and SWP observations were made, the mean SWP continuum is plotted against the mean LWR/P continuum in Figure 5. Some dependence with phase may be detected. Observations with the LWR camera are plotted as open circles; these were all made between egress and periastron/secondary eclipse and show nearly equal LWR and SWP continua. Through the rest of the orbit, the LWP continuum tends to be higher than the SWP continuum, and a greater variety is seen in the flux ratio.

3.1. Pedestal Fluxes

While nearly all the absorption features in the strong shell spectrum of 28 Tau are seen in the LWR/P observations of VV Cep, the line depths show significant differences. Figure 6 compares two regions of the VV Cep spectrum to those of 28 Tau. The upper panel includes the Mg II *k* line. As pointed out by Hack et al. (1989), the flux at the core of the *k* line is indistinguishable from zero, due to circumstellar and interstellar absorption. Note that while many of the shell features in 28 Tau approach zero central intensity, the Mg II *k* line is the *only* line in this region of the spectrum of VV Cep to do so. All but the weakest shell lines in VV Cep have about the same central depth. This behavior is seen throughout the well-exposed LWR/P region. The lower panel of Figure 6 shows the region of Fe II multiplet 1. All the lines with near-zero central intensity belong to this multiplet. For the zero-volt lines, an interstellar contribution is probable, but for the other lines, with lower levels from 0.05 to 0.12 eV, this narrow, deep absorption must be circumstellar in origin.

Initially, we attempted to determine the value of this minimum shell line absorption, or "pedestal" flux, in the same way we determined the continuum, by taking the median value of the flux between two selected wavelength points. However, the wavelength ranges of this minimum flux were much narrower than the continuum regions, and the automated procedure did not give satisfactory results. Therefore, three regions of the LWR/P spectrum were selected for the determination of the pedestal flux because of the presence of a number of suitable lines: 2635–2665, 2780–2810, and 2960–2990 Å. The pedestal flux was estimated by drawing a straight line at constant value across plots of the spectra.

In general, this pedestal flux was nearly equal in the two longer wavelength regions, typically $\sim(2\text{–}4) \times 10^{-12}$ ergs s^{-1} cm^{-2} $Å^{-1}$ and about 0.7 times as strong in the 2635–2665 Å region. Shortward of this, the pedestal flux appears to decrease, but since the shorter wavelength portions of the LWR/P observations are so underexposed, no meaningful conclusions can be drawn. By the SWP region, any pedestal flux is $\lesssim 10^{-12}$ ergs s^{-1} cm^{-2} $Å^{-1}$ and cannot be definitively detected (nor ruled out) with the *IUE* observations.

While the strongest shell lines are seen in all observations, some of the weaker lines are no longer seen when the continuum weakens. Figure 7 compares an observation with a particularly well-developed shell spectrum to a spectrum with a particularly low continuum. Note how the shell lines only appear strongly when the continuum rises above the value of the pedestal flux.

The pedestal flux and the mean LWR/P continuum are plotted with phase in Figure 8 and against each other in Figure 9. As discussed in § 4.4, the shell lines are especially deep in the latest *IUE* observations. Except for these latest

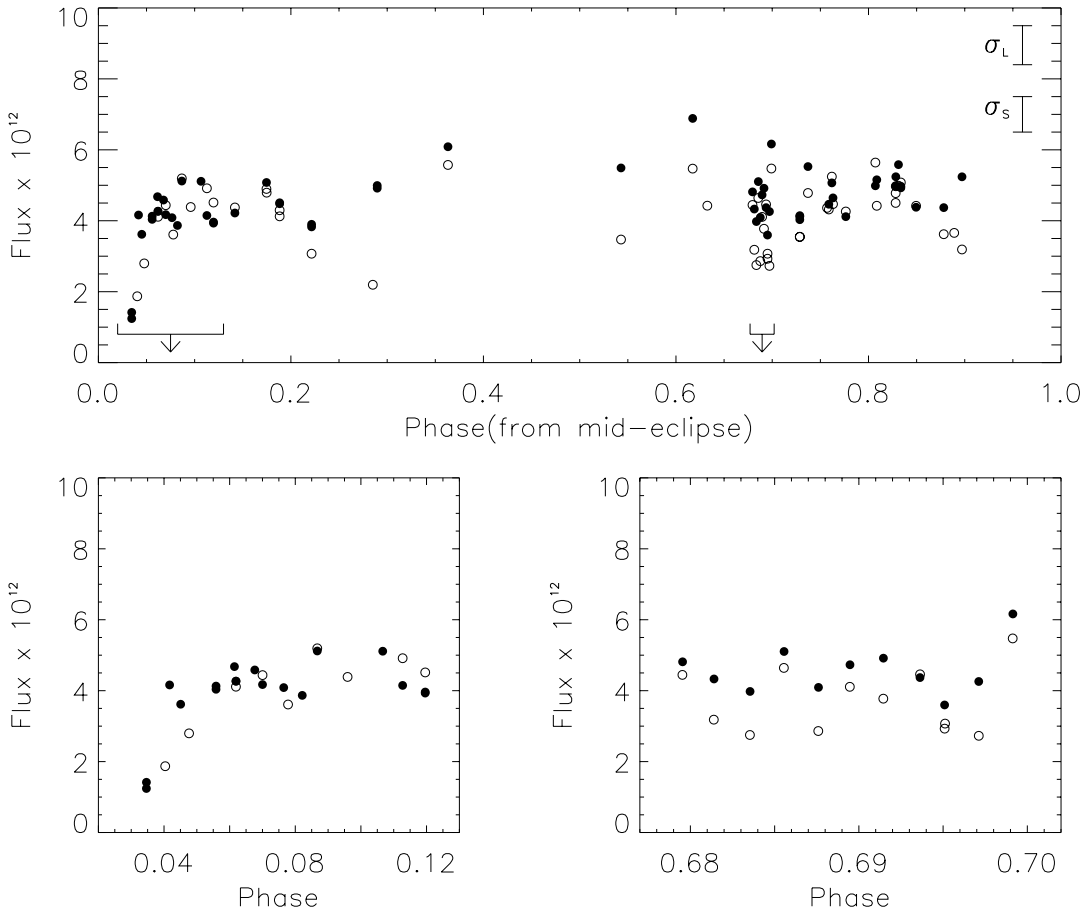

FIG. 4.—Continuum variation over the orbital cycle of VV Cep. Filled circles plot the continuum averaged over the LWR/P region and open circles the continuum averaged over the SWP region. (Wavelengths used in the averaging are shown as filled circles in Fig. 3). Because plotting the individual error bars would overly clutter the figure, the mean value for an error bar (± 1 standard deviation) for the LWR/P and SWP regions are plotted in the upper right of the upper panel. This standard deviation is that obtained when taking the mean of the continuum values at each wavelength. The SWP observations near $\phi = 0.29$ were obtained just over a month before the LWR observations. Thus the large difference between the LWR and SWP observations is likely to be a stochastic variation as opposed to an unusually "red" energy distribution. For clarity, regions in which observations were closely spaced in time (egress and the 1991 monitoring period) are plotted on an expanded timescale in the two lower panels.

observations, the pedestal flux and continuum tend to vary together.

4. THE ABSORPTION SPECTRUM

Throughout the entire orbital period, a rich absorption spectrum persists, although line behavior does depend on ionization state. High-ionization lines such as Si IV and Fe III are seen as broad features; these were described by Bauer et al. (1991) and will not be discussed further here. Neutral species with low ionization potential (e.g., Fe I) were seen to disappear as the hot component emerged from primary eclipse, while neutral elements with higher ionization potential remain in absorption. Lines arising from neutral elements are discussed in § 4.1. More complex behavior is shown by singly ionized elements; these are treated in the remainder of § 4. A general overview of the UV spectra of VV Cep and related objects is presented in §§ 4–6; the reader is referred to Table 2 for a detailed compilation of the appearance and behavior of prominent multiplets.

4.1. Neutral Elements

As noted in Bauer et al. (1991), some absorption lines from neutral elements are seen to weaken and eventually disappear as the hot component emerges from eclipse. However, some lines due to neutral elements do persist in the shell spectrum around the entire orbit. All unblended neutral lines in the 31 Cyg chromospheric eclipse spectra have been sought in the spectrum of VV Cep. Elements with enough observable lines for a conclusive determination of their presence or absence are discussed below in order of increasing ionization potential.

Fe I (IP = 7.9 eV) and S I (IP = 10.3 eV) both show numerous absorption lines during egress from chromo-

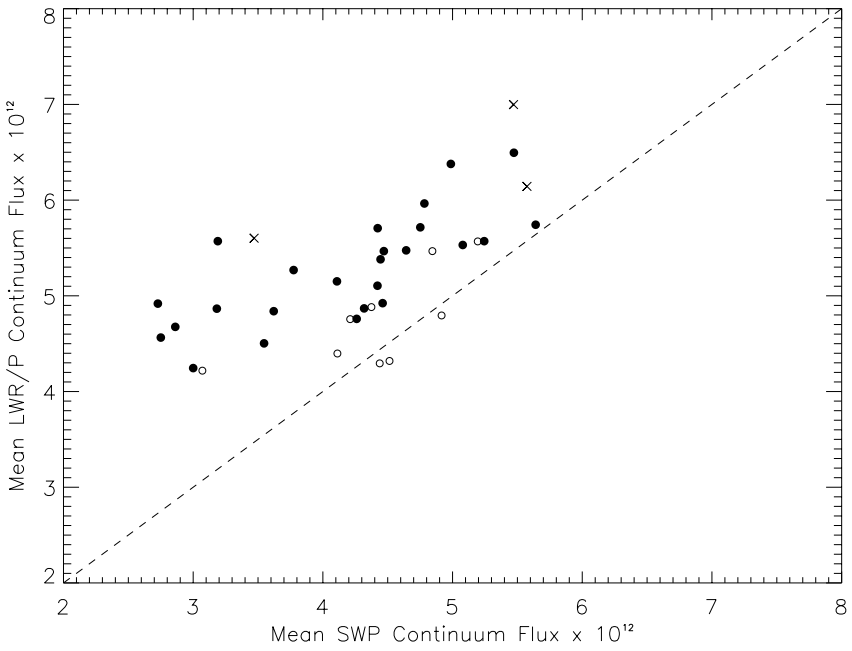

FIG. 5.—The continuum in the LWR/P region compared to that in the SWP region. LWR observations ($\phi \leq 0.290$) are plotted as open circles. The observation near periastron ($\phi = 0.363$) and the following two observations ($\phi = 0.543$ and 0.617) are plotted with crosses. The remaining LWP observations ($0.644 \leq \phi \leq 0.897$) are plotted with filled circles. The dashed line represents equal LWR/P and SWP continua. Egress from eclipse is not included in this figure because of the lack of contemporaneous SWP and LWR observations.

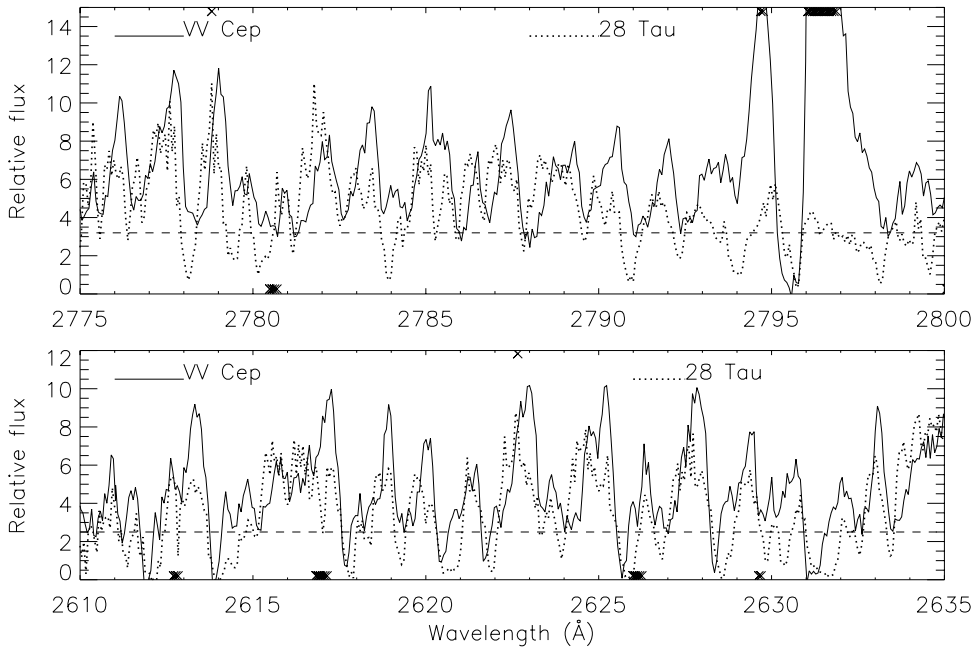

FIG. 6.—The pedestal flux and deep circumstellar lines in the spectrum of VV Cep. Selected regions of the spectrum of VV Cep (LWP 17446, 1990 March 1, $\phi = 0.617$) are compared to 28 Tau (LWR 5204, 1979 July 29) during strong shell phase. The dashed lines represent the minimum depth of shell lines as determined near 2785 and 2650 Å (see § 3.1). Fluxes for VV Cep are in units of 10^{-12} ergs s^{-1} cm^{-2} Å^{-1}. In the upper panel, Relative flux of 15 corresponds to 8×10^{-11} ergs s^{-1} cm^{-2} Å^{-1} for 28 Tau, and in the lower panel, Relative flux of 12 corresponds to 8×10^{-11} ergs s^{-1} cm^{-2} Å^{-1} for 28 Tau. Flagged data near 2617 Å in the LWR spectrum of 28 Tau are artifacts in the *IUE* intensity transfer function. The line at 2785 Å which is seen in absorption in 28 Tau but not in VV Cep is the strongest line of Fe II (373). This line was listed as an emission feature in the VV Cep spectrum by Hack et al. (1989), but an examination of all the spectra in this region shows no emission which is clearly higher than the continuum. However, this is a moderately strong shell line in 28 Tau, and its absence in VV Cep probably indicates that it is being filled in by emission.

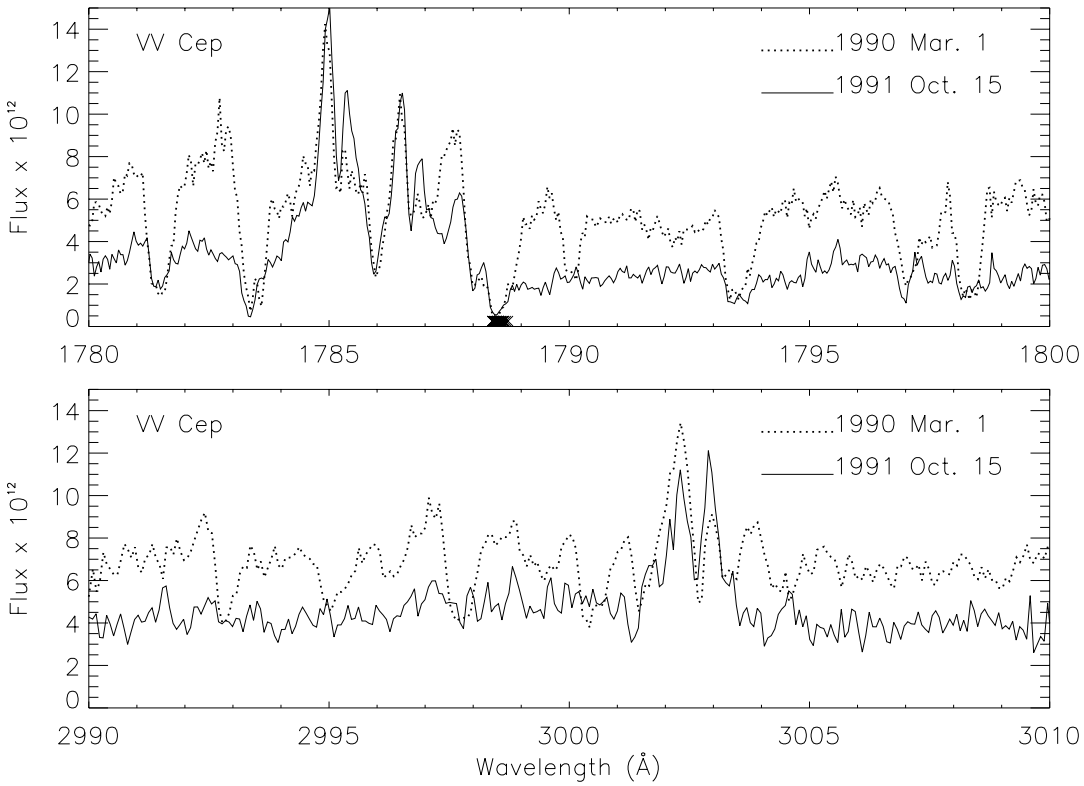

FIG. 7.—Variations in the continuum and strength of the shell spectrum. SWP 38281 (1990 March 1, $\phi = 0.543$) and SWP 42747 (1991 October 15, $\phi = 0.697$) are plotted in the upper panel, and LWP 17446 (1990 March 1) and LWP 21496 (1991 October 15) are plotted in the lower panel.

spheric eclipse. These lines disappear as the line of sight to the hot component moves through lower density regions higher in the M-star atmosphere, where neutral atoms are increasingly ionized because the photoionizing continuum is less shielded and recombination is less important. Even the zero-volt lines disappear.

C I has an ionization potential of 11.2 eV. Multiplets with lower levels of 0.00 or 0.01 eV remain in absorption throughout the entire orbit, and interstellar absorption is probable. There are a few unblended lines arising from 1.26 eV in the spectrum of 31 Cyg. These are missing from the out-of-eclipse spectrum of VV Cep, but do appear during egress. By the time the ionization potential has reached the 12.9 eV of Cl I, absorption persists around the whole cycle. Two of these lines have lower levels of 0.11 eV, probably too high for an interstellar origin.

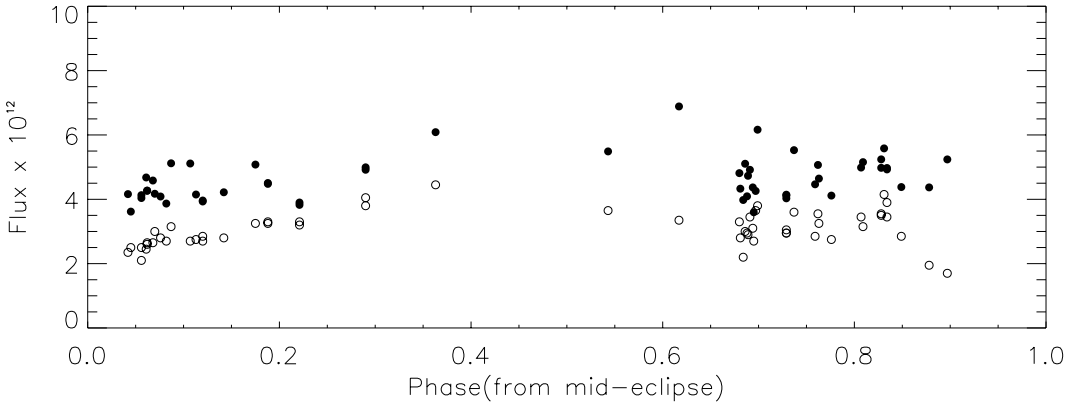

FIG. 8.—Mean LWR/P continuum and pedestal flux as a function of phase. The filled circles represent the continuum and the open circles the pedestal flux. Observations made during partial eclipse are excluded.

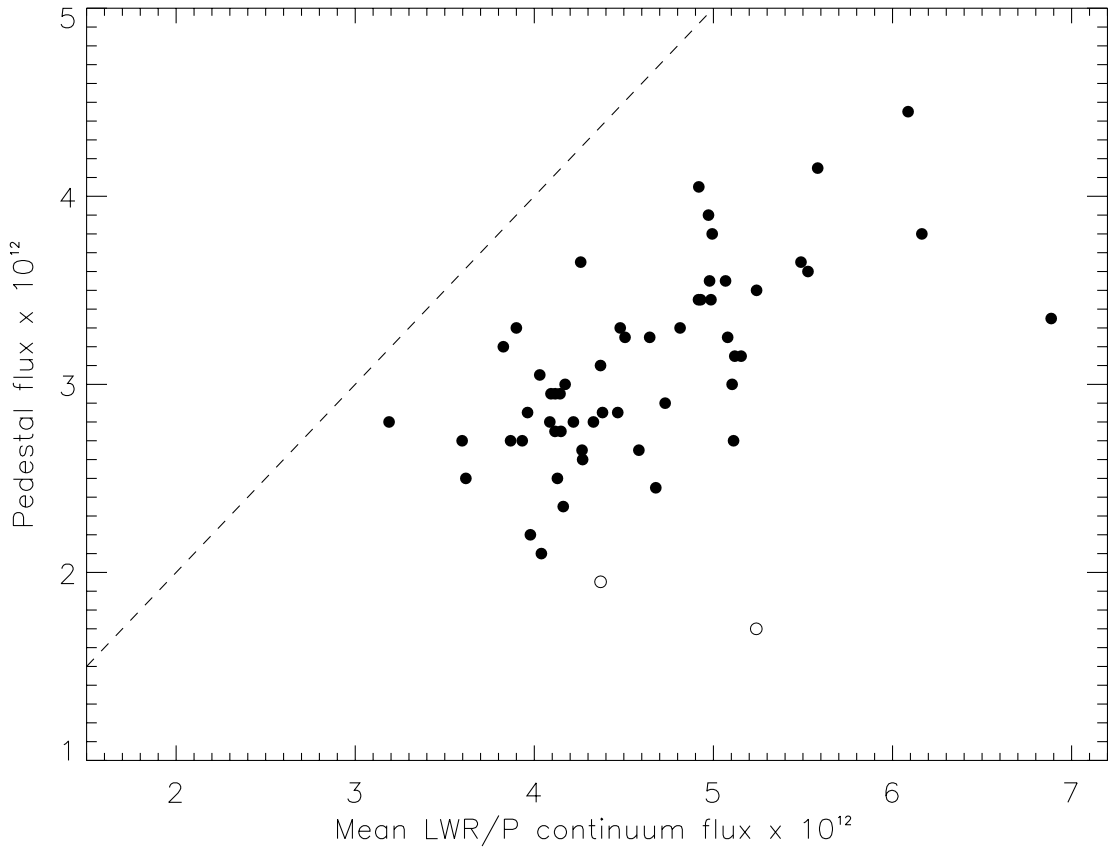

FIG. 9.—The ratio of the pedestal flux to the continuum flux. Open circles plot the observations made at $\phi = 0.878$ and 0.897 in which the shell absorption was especially deep (see § 4.4). The dashed line represents equal continuum and pedestal fluxes.

O I (IP = 13.6 eV) and N I (IP = 14.5 eV) both show some lines in absorption and some in emission; see § 5 and Table 2.

4.2. Singly Ionized Species

As discussed by Bauer et al. (1991), even far from eclipse, the UV spectrum of VV Cep is dominated by a rich absorption spectrum. A majority of these absorption lines are also seen in the spectrum of the ζ Aurigae star 31 Cyg as observed during chromospheric eclipse, and they are mainly due to singly ionized elements of the iron group. However, many of the absorption features in VV Cep are not seen in 31 Cyg; see the lines at ~1750.8, 1752.8, and 1753.6 Å in the upper panel of Figure 2. A much better match for the absorption spectrum of VV Cep is found in the spectrum of the Be-shell star 28 Tau. Nearly all the absorption features in the UV spectrum of VV Cep are matched by absorption features in the spectrum of 28 Tau as observed during strong shell phase. In the lower panel of Figure 2, the spectrum of VV Cep is compared to that of 28 Tau. Note that the absorption lines seen in VV Cep but not in 31 Cyg do appear in 28 Tau. Most of these lines that have thus far been identified arise from elements such as Cr II, Mg II, and Fe II and have higher excitation potential (~4–5 eV) than seen in 31 Cyg.

4.3. Circumstellar and Shell Lines

Lines of singly ionized species divide into two types: circumstellar and shell. As discussed in § 3.1 and shown in Figure 6, there is a minimum depth below which the shell lines in the spectrum do not absorb. The only exceptions are strong lines arising from low-excitation levels, as would be expected from the circumstellar envelope of an M supergiant. Multiplets in the well-exposed 2500–3000 Å region of the LWR/P spectrum which have lines with narrow absorption with lower central intensity than neighboring shell lines are Mg I (1), Mg II (1), Mn II (1), and Fe II multiplets 1, 62, 63, and 64. Note that the Mg, Mn, and some Fe II (1) lines are zero-volt lines and thus likely to have an interstellar contribution.

The rich shell absorption spectrum persists throughout the entire out-of-eclipse part of the cycle, but there are significant changes in the line profiles, which come as additional red- or blueshifted absorption seen in the shell lines (see Fig. 11 in Bauer et al. 1991 and Fig. 10 in this paper).

TABLE 2

LINE BEHAVIOR IN VV CEPHEI AND RELATED OBJECTS

Ion	Multiplet	Excitation Potential (eV)	Wavelength Range (Å)	VV Cep	HD 45677	α Sco	KQ Pup
C IV	1	0.00	1548–1551	h	h	h	h
Si IV	1	0.00	1393–1403	h	h	h	h
Al III	1	0.00	1854–1863	h	h	h	h
Fe III	34	3.73	1895–1927	h	h	x	h
Mg II	1	0.00	2795–2803	de	de	de	de
Si II	1	0.00–0.04	1808–1818	c, e	s	P	Pd, vr
Ca II	4	1.69	1838–1841	e	x	x	e
Cr II	5	1.48–1.54	2835–2879	c	P, s	x	Pd
Cr II	6–8	1.48–1.54	2653–2767	c	s	x	Pd
Mn II	1	0.00	2576–2606	c	s	c	Pd
Mn II	5	1.17	2933–2950	c	P, s	c	Pd
Fe II	1	0.00–0.12	2585–2632	c	s	P	Pd, vr
Fe II	8	0.00–0.12	1608–1640	s	s	c	vr, s
Fe II	38, 42–45	0.23–0.38	1550–1727	s	s	c	s
Fe II	60	0.98–1.07	2907–2980	e, c	P, s	P	Pd
Fe II	61	0.98–1.07	2861–2893	c	re	x	P
Fe II	62–63	0.98–1.07	2692–2773	e, c	P, s	P	Pd
Fe II	64	0.98–1.07	2562–2612	c	P, s	c	Pd
Fe II	78	1.66–1.72	2944–3003	c	P, s	x	Pd
Fe II	171	2.79–2.84	2608–2632	c	s	x	Pd
Fe II	177	2.79–2.84	2529–2556	c	s	x	a, P?
Fe II	191	2.88	1785–1788	e, c	P	ce	e
Fe II	234	3.23–3.25	2779–2798	c	s	x	Pd
Fe II	235	3.23–3.25	2753–2768	e, c	s	x	Pd
Fe II	263	3.37–3.41	2645–2667	c	s	x	a
Fe II	283	3.75–3.80	2657–2692	c	s	x	Pd
Fe II	373	5.18–5.24	2746–2797	f	s	re	e
Fe II	399	5.49–5.58	2824–2885	f	re, s?	x	e
N I	9	3.56	1742–1746	e	ce	x	pe
N I	10	3.56	1411.9	f	ce	x	pe
N I	11	3.56	1326–1328	a	f	x	pa
N I	12	3.56	1319–1320	a	s	x	pa
O I	2	0.00–0.03	1302–1307	e, c	P	c	Pd, vr
O I]	146	1.97	1641.3	e	ce	x	pe
Mg I	1	0.00	2852.1	c	a	c	c

NOTE.—Symbols used in table:

a: absorption. In VV Cephei, data are too noisy to determine whether lines behave as circumstellar or shell absorption. In HD 45677, a single strong absorption feature is seen; if shell absorption is present, the additional absorption component is weak.

c: circumstellar. In VV Cephei, a narrow absorption component is seen, which does not share the variable red- and blueshifted absorption seen in the shell lines. The line profile may well be affected by surrounding emission. In α Sco, a narrow absorption feature is seen. In KQ Pup, deep, narrow absorption is seen below the continuum in the 2600–3000 Å region.

ce: emission approximately centered on the systemic wavelength.

de: double-peaked emission with a strong central absorption component.

e: emission in at least one line of the multiplet.

f: feature is probably filled in with emission.

h: absorption feature due to the hot component.

P: P Cygni profile in at least one line of the multiplet.

pa: in KQ Pup, absorption which appears only near periastron.

Pd: in KQ Pup, the line profile is a P Cygni profile except near periastron, when a double-peaked emission profile is seen.

pe: in KQ Pup, emission which appears only near periastron.

s: shell absorption. In VV Cephei, these features show variable red- or blueshifted emission. In HD 45677, an absorption feature is always seen near the systemic velocity, and in most observations, an additional blueshifted component is also seen. In KQ Pup, variable additional redshifted absorption develops in the three observations nearest periastron.

vr: in KQ Pup, an additional redshifted component comes and goes throughout the entire observed portion of the cycle.

x: feature is not seen.

The VV Cep spectra shown in Figures 2 and 6 are from the observation of 1990 March 1, which was a "clean" spectrum, in which the shell lines were symmetric and the continuum strong. However, the continuum and the line profiles can vary independently of each other. Each panel of Figure 10 shows a pair of observations separated by about 2 weeks. In the upper panel, the continuum remains roughly unchanged, but over the 2 week time span between the two

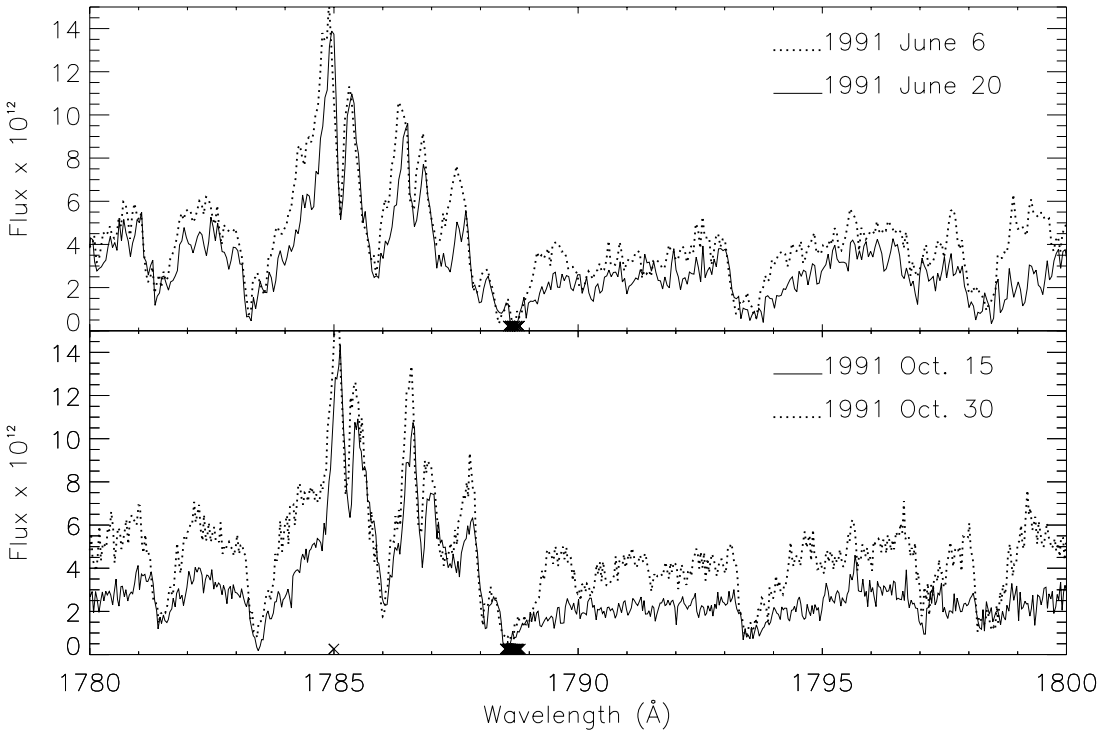

FIG. 10.—Rapid variations in the continuum and line profiles in VV Cep. SWP 41782 (1991 June 6, $\phi = 0.680$) and SWP 41886 (1991 June 20, $\phi = 0.681$) are plotted in the upper panel, and SWP 42727 (1991 October 15, $\phi = 0.697$) and SWP 42942 (1991 October 30, $\phi = 0.699$) are plotted in the lower panel. The lower panel is plotted with SIPS data, as SWP 42942 had not been processed with NEWSIPS at the time of writing.

observations plotted, the shell lines have developed additional redshifted absorption. Between the two observations plotted in the lower panel, the change over the 2 week interval is mainly in the continuum.

The majority of the spectra obtained show line profiles with additional redshifted absorption features. "Clean" spectra and additional blueshifts are much less common. The nature of the observed line profiles does not seem to be phase dependent. Figure 12 in Bauer et al. (1991) shows the distribution of "clean" spectra and spectra with additional red- and blueshifts observed in the SWP observations obtained through 1990 March 1. (The SWP observations are best for assessing the line profiles due to the lesser contamination by emission.) Since that time, SWP observations have been made on 29 different dates, 26 of which have shown additional redshifted absorption in the shell lines. The observation of 1993 January 14 was the only one to show additional blueshifted absorption, and the 1994 January 10 observation was the only "clean" spectrum. In the 1992 June 5 observation, the shell lines were roughly symmetric but broader than those observed in typical "clean" spectra.

The circumstellar lines discussed above do not show the line profile variations seen in the majority of the shell lines. There are also many other narrow absorption lines which do not share the line profile variations but which do not

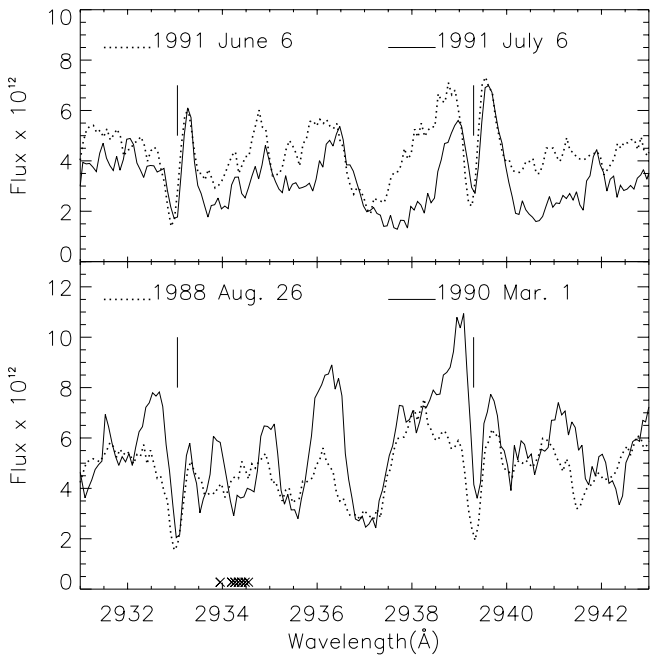

FIG. 11.—Circumstellar lines in the spectrum of VV Cep. In the upper panel, LWR 20533 (1991 June 6, $\phi = 0.680$) is plotted with LWR 20755 (1991 July 6, $\phi = 0.684$). In the lower panel, LWP 13918 (1988 August 25, $\phi = 0.543$) is plotted with LWP 17446 (1990 March 1, $\phi = 0.617$). Solid vertical lines mark the rest wavelengths of lines of Mn II (5).

have such low central intensities. Figure 11 compares four observations of VV Cep of a region of the spectrum which includes two lines of Mn II (5), whose wavelengths are marked by vertical lines. Note the sharp absorption feature present in both lines in all four observations.

Two spectra obtained during the 1991 monitoring period are plotted in the upper panel of Figure 11. They differ mainly in the strength of their additional redshifted absorption. In the nearly line-free region from 3007 to 3013 Å, the continua in these two spectra are quite close to each other (4.4 and 3.9 $\times$ 10^{-12} ergs s^{-1} cm^{-2} $Å^{-1}$ for the June and July observations, respectively). Note that the extra redshifting seen in the other shell lines is not present in the Mn II (5) features.

A well-developed shell spectrum, that of the "clean" spectrum of 1990 March 1, is plotted with the solid line in the lower panel. The Mn II (5) lines show the same narrow absorption. The additional redshifts in the upper panel can be seen by noting how the short-wavelength edges of the shell lines in this spectrum are aligned with those in the upper panel. The dotted line in the lower panel represents the observation of 1988 August 25, an unusual observation in which nearly all emission was reduced to the level of the continuum and shell lines showed strong additional blueshifted absorption. The shell lines are present as broad features, while the Mn II (5) lines retain their narrow appearance. The similarity of these narrow features to the lines with low central intensity suggests that they, too, originate in the M-supergiant wind.

Lines (in well-exposed regions of the spectra) which show this narrow, circumstellar profile without additional red- or blueshifted absorption arise from Fe II (1, 60, 61, 62, 63, 64, 78, 171, 177, 234, 235, 263, 283), Cr II (5, 6, 7, 8), Mn II (1, 5), Mg I (1), and Si II (1). Many of these narrow lines, most notably some of the Fe II and Cr II multiplets and Si II (1), are embedded within emission, which likely controls the overall profile.

4.4. The Spectrum Near Phase 0.9

The latest observations obtained by the *IUE* satellite show differences from those over the rest of the cycle: emission tends to be reduced, the shell lines are more redshifted relative to the circumstellar lines, and absorption in both the shell and circumstellar lines is deeper. These changes are illustrated in Figure 12, in which a region of the latest LWP *IUE* observation of VV Cep is compared to the "clean" observation of 1990 March 1.

First, the shell spectrum is unusually well developed in both of these spectra; more often the shell lines in this region of the spectrum (which arise from Cr II, Fe II, and Ni II with excitation potential between 3 and 5 eV) are very weak or absent, as seen in the 1991 October 15 observation plotted in Figure 7. While these shell lines can be seen at

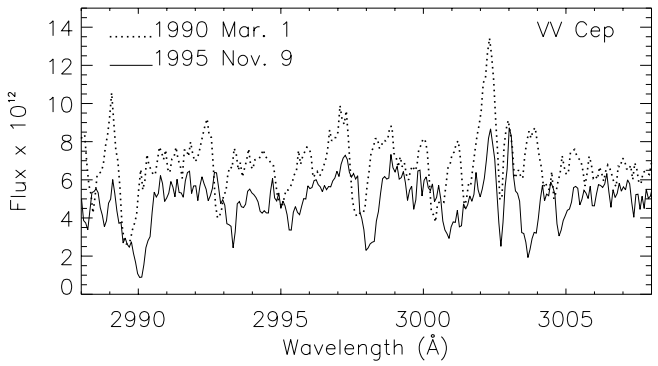

FIG. 12.—The spectrum of VV Cep near phase 0.9. The dotted line plots the "clean" spectrum of 1990 March 1 (LWP 17446; $\phi = 0.617$). The last *IUE* LWP observation of VV Cep (LWP 31678, $\phi = 0.897$) is plotted with a solid line. The $\phi = 0.897$ observation is displaced by +20 km s^{-1} in order to line up the circumstellar absorption feature in the 3002.646 Å line of Fe II (78).

phases spread around the orbit, their strongest occurrences are in observations near primary eclipse (the first three observations after partial eclipse, LWR 1525, 1673, and 1807, and the last two observations made as the system approached ingress) and in the observation made near periastron/secondary eclipse and the following two observations, which were made near third quadrature. However, the radial velocity of the shell lines relative to that of the circumstellar lines is quite different in the latest *IUE* observations than around the rest of the cycle. In Figure 12, the wavelength scale has been adjusted so that the circumstellar components of the 3002.646 Å line of Fe II (78) line up, and the shift in the radial velocity of the shell features relative to this circumstellar feature is clearly seen.

Both the circumstellar and shell absorption features have greater central depth in the last two LWP observations. Many shell features penetrate below more typical values of the pedestal flux, although the values of the continuum are not at all unusual.

Weak circumstellar lines in particular look stronger in these latest *IUE* observations. See Figure 1; note that these observations have the longest path through the primary's atmosphere.

This increased line absorption does not appear to be the beginning of ingress into primary eclipse, as the absorption by low-ionization neutral species has not yet begun.

4.5. Radial Velocities

Radial velocities were measured in the LWR/P region for two of the line components: shell and circumstellar lines. Shell lines were selected for measurement only if they were present in the spectrum of 28 Tau but not 31 Cyg, in the hope that such lines would be formed in a more homogeneous region than those over a greater range of excitation

potential. Blended lines were rejected on the basis of a computer program which predicted absorption-line strengths in a slab of given column density and temperature using Kurucz's (1990) line list. A sample of 13 shell lines was used. A total of 31 circumstellar lines were selected; no zero-volt lines were used in order to exclude contamination by interstellar absorption.

A total of 22 images were selected in which the shell lines were prominent enough to make a reasonable measurement. Circumstellar lines were measured in all decently exposed spectra. The wavelength region over which to measure the line radial velocity was selected interactively, and a parabola was fitted to the data points within the selected line profile. The centroid of the parabola was adopted as the observed wavelength.

The mean radial velocity of the circumstellar and shell lines are plotted for each phase along with Wright's (1977) radial velocity curve for the two stars in Figure 13. Neither of these line components appears to follow either of the two stars.

Most of the circumstellar line measurements range from approximately the systemic velocity of -20 km s^{-1} to about ~ 15 km s^{-1} more negative, consistent with their formation in an expanding circumstellar envelope which is large compared to the scale of the orbit.

The larger error bars for the shell line measurements result from several factors. There were fewer measured lines, and they tended to be weaker; some misidentified lines may be included. In addition, these shell lines show stochastic profile variation, with additional red- or blueshifted absorption. Although the spectra with the most extreme additional redshifts were omitted, this must affect the results. For example, the observations at $\phi = 0.363$ and 0.617 both showed additional redshifts, and that at $\phi = 0.543$ showed additional blueshifting, and the measured radial velocity for the shell lines in the $\phi = 0.543$ observations is less than that for the observations at $\phi = 0.363$ and 0.617.

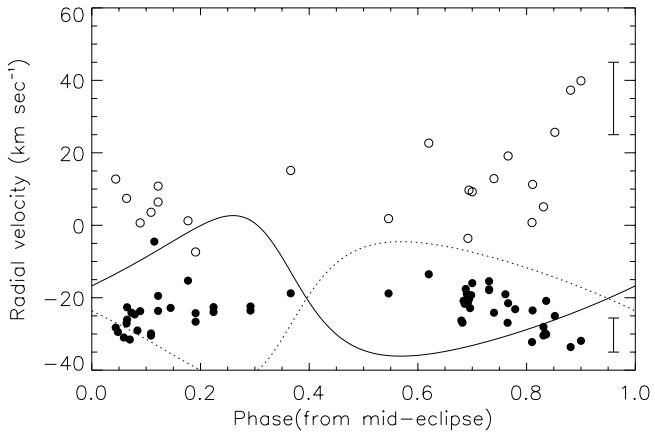

FIG. 13.—Radial velocities of the circumstellar and shell lines. Filled circles represent circumstellar lines and open circles represent shell lines. Wright's (1977) radial velocity curve for the system is plotted; the solid line represents the M supergiant and the dotted line the hot component. The error bars in the upper and lower left represent the mean error (± 1 standard deviation) for the shell and circumstellar lines, respectively. The circumstellar-line radial velocity near -5 km s^{-1} was measured for LWR 6221. The NEWSIPS processing for this image appears to have a radial velocity shift from the SIPS data; remeasured with the SIPS data, this value was -20 km s^{-1}.

The radial velocities of the two components are noticeably different on the plots of the latest *IUE* observations, with the shell lines clearly more redshifted relative to the circumstellar lines than throughout the rest of the cycle. As discussed in § 4.4, absorption in the shell lines is also deeper in these observations.

5. THE EMISSION SPECTRUM

A major feature of the out-of-eclipse spectrum of VV Cep is the presence of numerous emission lines, mostly due to various multiplets of Fe II. A detailed listing of the emission spectrum and a discussion of potential excitation mechanisms were given by Hack et al. (1989).

In general, emission lines remain in emission throughout the orbital cycle as observed by *IUE*. There are two notable exceptions, both discussed by Bauer et al. (1991, and shown again in Fig. 14): First, in the earliest LWR spectrum, obtained during partial eclipse, only the long-wavelength peak of double-peaked Fe II emission is yet visible. This emission may come from the wind of the M supergiant as it is illuminated by the B star and may well be present during totality. Second, in an observation made 1988 August 25, just before third quadrature, nearly all the emission was reduced to at least the level of the nearby continuum.

The strongest lines in the emission spectrum, the *h* and *k* lines of Mg II, always appear as a double-peaked emission feature with a central core whose intensity is indistinguishable from zero. Representative profiles are plotted in panels *a*–*e* of Figure 14. Throughout most of the cycle, the long-wavelength emission peak was roughly twice as strong as the short-wavelength component, and the *k* line was stronger than the *h* line. The emission strengthened as the stars approached periastron, with the red and blue peaks more nearly equal and the *h* and *k* lines having roughly the same strength. The observation made closest to periastron, on 1984 December 28, was severely overexposed in the *h* and *k* lines, and is thus not included in Figure 14, but the emission was at least as strong as that observed at $\phi = 0.290$. Periastron and secondary eclipse occur at very nearly the same phase. Two factors could be contributing to the increase in emission observed at this time: first, we are seeing a greater fraction of the half of the M supergiant which is illuminated by the hot star, and second, the hot star is closer to the cool star and thus likely embedded in a denser portion of the M-star wind.

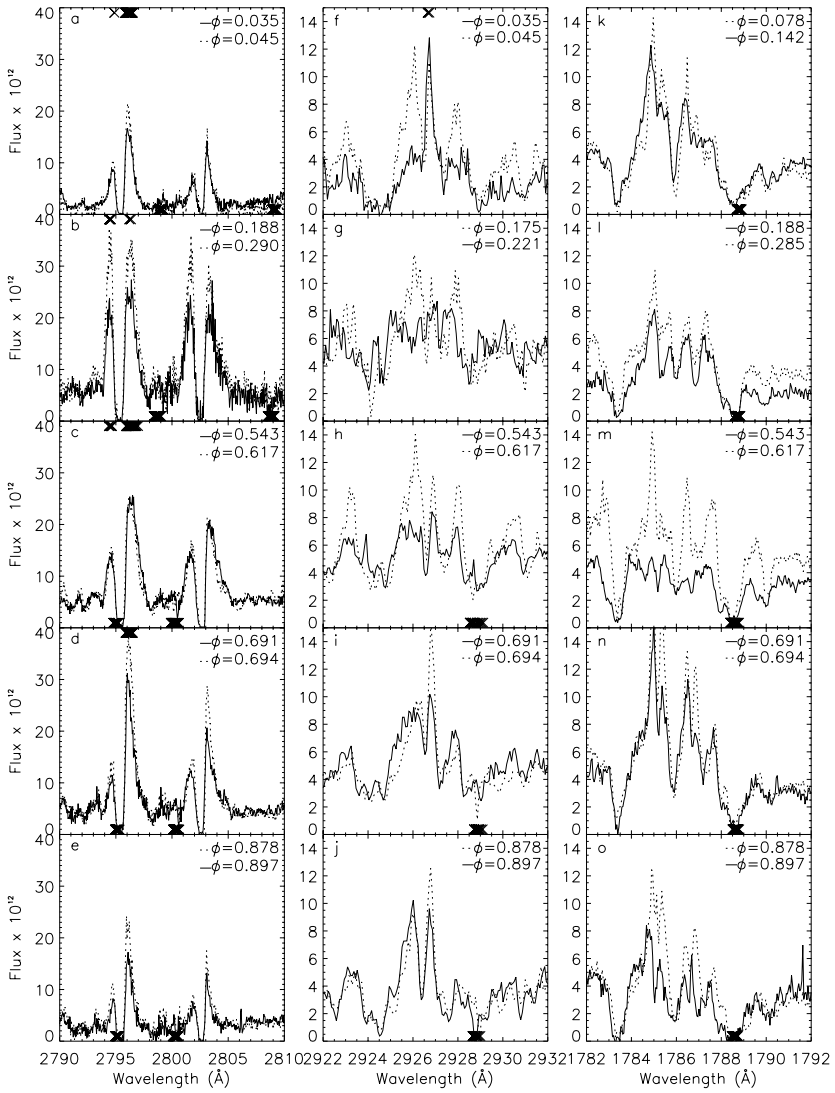

FIG. 14.—Variation of emission lines with phase. Panels *a–e* (the Mg II *h* and *k* lines) were plotted using SIPS data. These lines were overexposed in most observations. The SIPS processing was chosen for these lines because it better reproduced the *h* and *k* line shapes seen in images in which they were not overexposed. Panels *f–j* plot the 2926.585 Å line of Fe II (60), and panels *k–o* plot Fe II (191).

In addition to this phase-dependent behavior, relatively rapid variations in the intensity of the *h* and *k* lines occasionally occur. Panel *d* in Figure 14 shows the Mg II *h* and *k* lines as observed 2 weeks apart, on 1991 September 3 and 19. The emission, particularly in the long-wavelength peak of both lines, strengthened considerably over this relatively short time interval. The emission was still this strong in the observation of 1991 October 1, but by October 15, it had decreased to the level of the September 3 observation.

The second and third columns of Figure 14 show emission lines of Fe II as observed at different phases. However, there is very little phase dependence seen in these lines and considerable stochastic variation. Panels *f–j* show the 2926.585 Å line of Fe II (60). Panel *f* shows the only obvious phase dependence seen in this line, that the emission peak is single during partial eclipse (1978 April 23). By 1978 May 25, a shorter wavelength peak had emerged. Bauer et al. (1991) suggested that this line might actually be triple peaked, consisting of a narrow central circumsystem peak, with emission peaks on both sides, resulting from the disk around the hot companion. However, in the spectrum of KQ Pup there is an emission feature at the position of the longest wavelength of the three possible components, attributed to Mg II (2) by Altamore, Giangrande, & Viotti (1982). The distinct dip between the narrow circumsystem component and this longer wavelength emission result from a shell absorption line seen in 28 Tau but not 31 Cyg, preventing its recognition as an absorption feature in the earlier work.

Throughout the cycle, the two emission peaks of the Fe II

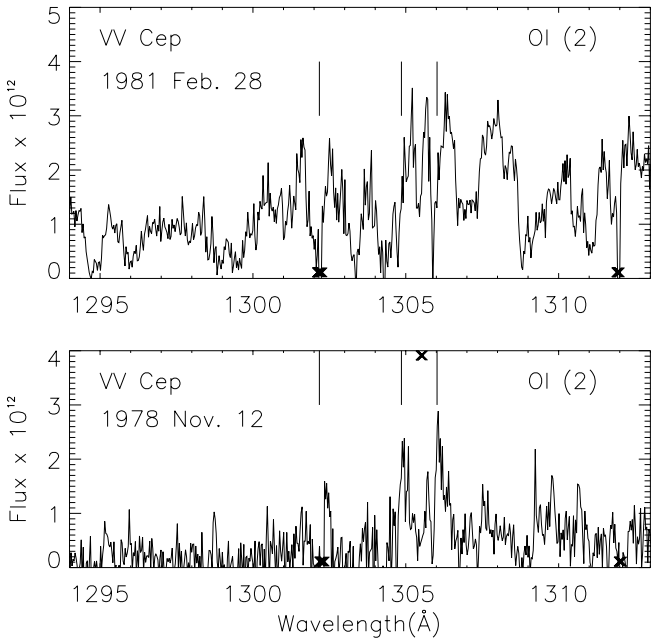

FIG. 15.—The region of O I multiplet 2 in VV Cep. The spectrum in the lower panel was taken during egress from eclipse (SWP 3322, $\phi = 0.062$) and that in the upper panel was taken near first quadrature (SWP 13383, $\phi = 0.175$). Vertical lines mark the wavelengths of the three lines of the multiplet. In the 1978 November 12 spectrum, a bright spot near 1306 Å left a spike, which has been removed by interpolating between the data points on either side; the affected data are marked with crosses above the spectrum.

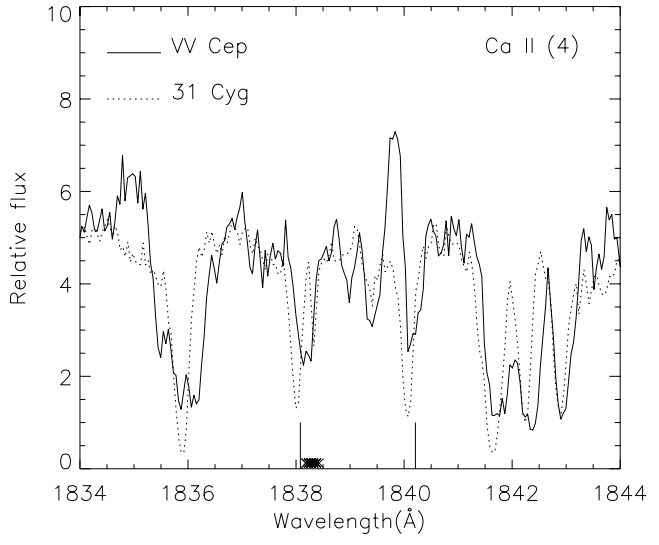

FIG. 16.—Emission in Ca II (4) in VV Cep. The solid line is the spectrum of VV Cep, SWP 38281, observed 1990 March 1 ($\phi = 0.617$); the dotted line is 31 Cyg as observed during chromospheric eclipse on 1982 September 3, SWP 17845. The two solid vertical lines mark the positions of the two lines of Ca II (4). Fluxes for VV Cep are in units of 10^{-12} ergs s^{-1} cm^{-2} Å^{-1}. Relative flux of 10 corresponds to 1.7×10^{-10} ergs s^{-1} cm^{-2} Å^{-1} for 31 Cyg.

(60) line are almost always seen, with varying intensity, and their variations are followed by numerous other Fe II lines. In a very few observations, e.g., $\phi = 0.221$ and 0.543 as shown in panels *g* and *h*, the emission is significantly reduced. This is only observed at times when the shell lines show additional blueshifted absorption. The rapid variation in the Mg II lines in 1991 September is also seen in this line, and in Fe II (191), as shown in panels *i* and *n*.

The strongest emission features in the SWP region arise from multiplet 191 of Fe II, and the appearance of the spectrum in this region is severely affected by numerous shell lines. A single emission peak from each of the three lines is seen at only two times: 1981 February 27 and 28 ($\phi = 0.175$) and 1990 March 1 ($\phi = 0.617$, plotted in panel *m* of Fig. 14). At both of these times, the spectrum was "clean"; i.e. lines in the shell spectrum were strong and symmetric. There were no well-exposed SWP observations made at an epoch early enough to show only a circumsystem component. Panels *k*, *n*, and *o* of Figure 14 show typical observations of this region. In some of the observations, weak emission from the longest wavelength line is seen, but the two stronger, shorter wavelength lines are often the only emission seen. Usually the emission is double peaked, with a central absorption whose wavelength corresponds to the circumstellar lines (e.g., $\phi = 0.078$ in panel *k* and all the spectra in panels *n* and *o*). The profiles of these two components vary together.

Most of the variation in Fe II (191) appears to be stochastic in nature. The only potential phase dependence in is seen in panel *l*. SWP observations of VV Cep were only made on three dates in this portion of the orbit (1981 June 8, $\phi = 0.188$; 1982 February 10, $\phi = 0.222$; and 1983 May 28, $\phi = 0.285$), and all these observations show this four-peaked structure. On the first two of these dates, the shell lines showed blueshifts. The 1983 May 28 observation had an unusually low continuum, and the shell lines are not well exposed, but appear fairly symmetric.

Reasonable exposures of O I multiplet 2 near 1300 Å are available only for the three longest SWP exposures; two of these are compared in Figure 15. SWP 3322 was obtained on 1978 November 12, still within chromospheric eclipse, and the continuum at 1300 Å is still significantly depressed. Only in this observation is the 1302.169 Å line clearly seen in emission. All three components are visible, although not in the expected intensity ratio (see Hack et al. 1989). By the time of the next long SWP exposure, made on 1981 February 28 (near first quadrature), the continuum has risen to the point where the emission no longer clearly stands out. Instead the appearance of the region of the longer two lines is dominated by two sharp absorption features, one of which is probably due to the 1306.029 Å line of O I. The other is probably due to P II (2) 1305.531 Å and/or Si II (13.04) 1305.590 Å. The presence of the other lines of these multiplets cannot be conclusively confirmed because they

lie in severely blended regions of the spectrum. However, a significant contribution from the P II (2) line is likely because strong absorption from P II (1) is clearly present near 1540 Å. The final long SWP exposure (made 1994 June 15) looks similar to the 1981 exposure.

Hack et al. (1989) discussed the N I (9) emission line at 1745 Å (see Fig. 2, in which the wavelengths of the two lines of this multiplet are marked with solid vertical lines). They noted that this is the weaker line of the two in the multiplet, and that multiplet 4, composed of stronger lines which share the same upper level, is seen in absorption and attributed this to the 1745 Å line not showing self-absorption, while the others do. However, examination of many observations of the N I (9) lines makes it apparent that the 1742 Å line is also in emission, as it follows the profile variation of the 1745 Å line. Both lines often show central absorption components, and their profile variations tend to follow those of Fe II(191).

The 1840.06 Å line of Ca II also appears in emission in many of the spectra of VV Cep. The emission is weaker than that of N I (9) and was not listed by Hack et al. (1989). It is best seen when the VV Cep spectrum is compared to the chromospheric eclipse spectrum of 31 Cyg, as shown in Figure 16. This is a similar situation to N I (9) in that the lower levels of the multiplet are metastable, and the longer wavelength component is the one showing the stronger emission.

6. STARS WITH RELATED UV SPECTRA

6.1. 28 Tau

28 Tau (Pleione of the Pleiades) is a variable B star, which has sometimes shown a normal B8 V spectrum, sometimes a Be spectrum, and sometimes a Be-shell spectrum. The star underwent a luminosity drop in 1973, and shortly thereafter, a strong shell spectrum developed. Doazan, Thomas, & Bourdonneau (1988) described the UV spectrum as it changed from the strong shell phase in 1979–1981 through the weakening of the shell spectrum in the late 1980s. The strong shell spectrum of 1979–1981 consists almost entirely of shell absorption features, mostly arising from singly ionized elements. Unlike VV Cep, no emission or high-ionization (e.g., Si IV, C IV) absorption features are seen, although the high-ionization lines did appear as the shell spectrum weakened. The lines of Fe I and S I which disappeared as the hot component of VV Cep came out of eclipse are seen in the strong shell spectrum of Pleione, although they are weaker than in the chromospheric eclipse spectrum of 31 Cyg.

Nearly all the absorption features in the VV Cep spectrum (except the high-ionization lines) are seen in the 28 Tau strong shell spectrum. However, the 28 Tau lines are much narrower than their shell counterparts in the VV Cep spectrum but are comparable in width to the VV Cep circumstellar absorption features. As discussed in § 3.1, the central depths of the absorption features are different between the two objects, with many of the shell lines in 28 Tau absorbing to near-zero central intensity, while absorption in these lines in VV Cep does not go below the "pedestal" flux. The weakest shell lines in 28 Tau are not seen in VV Cep, but this may simply be due to their increased breadth and the noise level in the spectra.

6.2. HD 45677

The B[e] star HD 45677 provides an interesting spectral analog to VV Cep because nearly all the same emission features are seen in the two objects. The B[e] designation comes from forbidden emission lines observed in the optical spectrum, another feature in common with VV Cep. Although the star is not associated with any visible nebulosity, Grady et al. (1993) classify it as a Herbig Ae–Be star because of their detection of accreting gas in the UV spectrum. However, other researchers believe that it may be a post–main-sequence star; for a discussion of the uncertainty in its evolutionary status see de Winter & van den Ancker (1997).

Early *IUE* observations of HD 45677 were discussed by Stalio & Selvelli (1981). HD 45677 continued to be observed through 1995, and we have examined high-resolution spectra from all observed epochs. Spectra taken between 1979 and 1990 show a lower continuum and more pronounced emission lines than those taken between 1993 and 1995; comparisons of the emission spectrum with VV Cep are made from the earlier spectra with the more prominent emission lines.

While nearly all the same emission lines are seen in HD 45677 and VV Cep, the radial velocity structure of the lines is very different. In VV Cep, the strongest emission in most lines is blueshifted. Most of the emission lines in HD 45677, however, show P Cygni profiles or are redshifted. Although the two objects must have regions of similar density and temperature, the B[e] phenomenon must have a different origin.

A further similarity between the UV spectra of HD 45677 and VV Cep is the presence of a shell absorption spectrum. However, the shell absorption spectrum in HD 45677 is much weaker than in VV Cep or 28 Tau during strong shell phase. In most observations, there was additional blueshifted absorption associated with the shell lines. Sometimes the shell lines are clearly doubled, while at other times the two components merge, giving rise to the "blocky" shell absorption profiles noted by Grady et al. (1993). The additional absorption in HD 45677 always has a sharp short-wavelength edge, while in VV Cep, the extra absorption is spread over a greater range of velocities.

6.3. α Sco

α Sco is a useful comparison for VV Cep because it consists of an M1.5 Iab–Ib supergiant with a B4 Ve companion. The light from the B star shines through the M-supergiant wind. However, the separation of the two stars is much greater than that for VV Cep: the projected separation of the two stars is about 520 AU, and the B star is probably about 780 AU closer to us along the line of sight than the M star (van der Hucht, Bernat, & Kondo 1980). This leads to a true separation of about 940 AU, as opposed to the *maximum* separation of 34 AU for the components of VV Cep. Despite the fact that the B star shines through much less of the M-star wind, the UV spectrum of α Sco does show some of the same features as that of VV Cep. Three of the five components of the VV Cep spectrum are seen in α Sco: emission lines, broad hot-star absorption lines, and narrow circumstellar/interstellar absorption. However, the emission and absorption spectra are considerably less intense than in VV Cep. The lines in the sharp circumstellar/interstellar absorption spectrum of α Sco are listed by Bernat (1982). As pointed out by Hagen, Hempe, & Reimers (1987), lines arising from excited levels show P Cygni profiles, but zero-volt lines do not because interstellar absorption wipes out the emission component.

6.4. KQ Pup

KQ Pup has been classified as a VV Cephei–type star based on its optical spectrum, which shows an M1–2 Iab star with a hot companion and forbidden emission lines. The orbital period is 27 years. The *IUE* observations miss the epoch of periastron. They are roughly symmetric around apastron, with the last few observations closer to periastron than the early observations were. Altamore et al. (1982) presented identifications for more than 600 absorption and emission lines and found two main line components: broad absorption features including high-ionization lines, and narrow P Cygni lines of neutral and singly ionized species. Rossi et al. (1992) present a model in which the optical and UV emission lines form in regions of the cool-star wind ionized by the hot companion, and the broad absorption lines form in material near to and approaching the hot star.

We have examined high-resolution spectra obtained at each *IUE* observation epoch. All components seen in the VV Cep spectrum are seen, with the exception of the neutral lines which appear only during VV Cep's chromospheric eclipse phase. KQ Pup is not known to be an eclipsing binary, and in any case, *IUE* missed the epoch at which the hot component would pass behind the M supergiant. KQ Pup has a more extensive emission spectrum than VV Cep, while VV Cep possesses a more extensive absorption-line spectrum.

Longward of 2600 Å the UV spectrum of KQ Pup has a definite flat continuum with almost no absorption lines. Other than very weak P Cygni absorptions associated with strong emission lines, the only lines seen in absorption arise from multiplets which are seen as circumstellar lines in VV Cep. Below 2600 Å, absorption lines become more prominent. In the SWP region, fewer emission lines are seen, and a shell spectrum similar in strength to that of HD 45677 dominates.

KQ Pup has a much more extensive emission-line spectrum than VV Cep. The intensities of many (but not all) of the lines in the LWP/R spectra are much stronger relative to the continuum in KQ Pup than they are in VV Cep. In the SWP region, emission-line intensities are more comparable between the two systems.

As shown by Rossi et al. (1997), many of the emission lines strengthen as the system approaches periastron, including the Mg II *h* and *k* lines. Unlike VV Cep, the orbit of KQ Pup is oriented with apastron near quadrature, rather than near conjunction, permitting us to compare spectra taken at similar separations, but with different amounts of the heated M-star hemisphere facing us. In KQ Pup, Mg II *h* and *k* emission strengthens both with decreasing separation and with viewing a greater portion of the heated M-star hemisphere, indicating that both effects probably contribute in VV Cep as well.

Rossi et al. (1997) note the broadening of the emission in Fe II (191) as KQ Pup approaches periastron. This is also seen in other strong lines of Fe II (e.g., multiplets 60, 62, and 78). Near apastron, these lines show narrow emission components with very weak P Cyg absorption. As the system approaches periastron, the lines appear as broader, double-peaked features. Although we have made no quantitative radial velocity measurements, the position of the central reversal appears very near that of the original P Cygni absorption, suggesting a circumstellar origin. For lines which do develop this double-peaked structure, stochastic variations are seen in the V/R ratios, similar to those seen in VV Cep. A complete discussion of this is beyond the scope of this paper. However, it should be noted that the profiles of strong Fe II emission lines in the observation of KQ Pup nearest periastron greatly resemble those of VV Cep.

In the SWP observations of KQ Pup, a shell absorption spectrum similar in strength to that of HD 45677 is seen throughout the cycle. In the three *IUE* observations nearest periastron, this spectrum strengthens and develops strong, variable additional redshifted components very similar to those seen in VV Cep.

7. SUMMARY

Even well out of eclipse, the UV spectrum of VV Cephei remains far more complex than those of the ζ Aurigae systems. Five line components have been identified:

1. Emission, some of which arises from the extended circumstellar envelope of the M-supergiant primary, and some of which forms close to the hot component.

2. Absorption lines from neutral species, many of which disappear as the hot component emerges from the chromospheric phase of the eclipse. Except for interstellar and/or circumstellar absorption, only neutral species with relatively high ionization potential (e.g., Cl I) are seen throughout the cycle.

3. Broad absorption from high-ionization species (e.g., Si IV, Fe III) which arises in the hot companion or in nearby hot circumstellar gas, which is possibly accreting onto the companion.

4. Shell absorption lines with variable profiles, so called because the same lines are observed in the strong shell phase of the Be star 28 Tau. In the LWR/P region, there is a minimum depth, or "pedestal," below which these lines do not absorb. This pedestal varies between observations from $\sim$35% to $\sim$85% of the continuum. Because of the rapid profile variation, at least some of this absorption must occur in material nearby (and probably accreting onto) the hot component.

5. Narrow circumstellar absorption lines which do not share the profile variations of the shell lines, and some of which absorb below the pedestal. These lines arise from strong, generally low-lying transitions and likely form in the extended circumstellar envelope of the M-supergiant primary.

The only emission lines whose variation is mainly phase dependent are the *h* and *k* lines of Mg II, which are stronger and broader near periastron/secondary eclipse. Variations in the other emission lines, both in intensity and in their profiles, are apparently stochastic in nature.

The continuum in both the LWR/P and SWP regions is highly variable, in an apparently stochastic manner. In one 2 week period in 1991, the SWP continuum value doubled, nearly spanning the entire range seen in the SWP continuum outside eclipse. The $\lambda^{-0.8}$ dependence of the continuum flux suggests that the source is not purely stellar.

Radial velocities were measured for both shell and circumstellar lines. Neither of these followed the radial velocity curve of either of the two stars. The circumstellar line velocities showed no variation within the expected errors in measuring radial velocities with *IUE* data and were consistent with their formation in the expanding M-star wind. The shell lines are always redshifted relative to the systemic velocity by about 30 km s^{-1}, with the latest *IUE* observations showing the greatest redshift. In the latest two LWP observations, made as the hot star approached ingress into primary eclipse, the shell lines are redshifted by $\sim$60 km s^{-1} from the systemic velocity and absorption in both the shell and circumstellar lines is deeper.

Partial support for this work was provided by NASA through grant GO-7269.01-96A from the Space Telescope Science Institute, which is operated by the Association of Universities for Research in Astronomy, Inc., under NASA contract NAS5-26555. This research used the SIMBAD database, operated at CDS, Strasbourg, France. W. H. B. would like to thank Tamarleigh Grenfell and Deanne Taylor for their help in accessing and plotting the *IUE* data in the early phases of this project.

REFERENCES

Altamore, A., Giangrande, A., & Viotti, R. 1982, A&AS, 49, 511
Bauer, W.H., Stencel, R. E., & Neff, D. H. 1991, A&AS, 90, 175
Bernat, A. P. 1982, ApJ, 252, 644
Cardelli, J. A., Clayton, G. C., & Mathis, J. S. 1989, ApJ, 345, 245
Cowley, A. P. 1969, PASP, 81, 297
de Winter, D., & van den Ancker, M. E. 1997, A&AS, 121, 275
Doazan, V., Thomas, R. N., & Bourdonneau, B. 1988, A&A, 205, L11
Grady, C. A., Bjorkman, K. S., Shepherd, D., Schulte-Ladbeck, R. E., Perez, M. R., de Winter, D., & The, P. S. 1993, ApJ, 415, L39
Guinan, E. F., McCook, G. P., Koch, R. H., & Pfeiffer, R. J. 1986, in Highlights of Astronomy: Volume 7, Proc. 19th IAU General Assembly, ed. J.-P. Swings (Dordrecht: Reidel), 211
Hack, M., Engin, S., & Yilmaz, N. 1989, A&A, 225, 143
Hagen, H.-J., Hempe, K., & Reimers, D. 1987, A&A, 184, 256
Hagen, W., Black, J. H., Dupree, A. K., & Holm, A. V. 1980, ApJ, 238, 203
Hjellming, R. M. 1985, in Radio Stars, ed. R. M. Hjellming & D. M. Gibson (Dordrecht: Reidel), 151
Kawabata, S., & Saito, M. 1997, PASJ, 49, 101
Kurucz, R. L. 1990, Trans. IAU, 20B, 169
Mollenhoff, C., & Schaifers, K. 1981, A&A, 94, 333
Nakagiri, M., & Yamashita, Y. 1979, Ann. Tokyo. Astron. Obs., 27, 147
Rossi, C., Altamore, A., Baratta, G. B., Friedjung, M., & Viotti, R. 1992, A&A, 256, 133
Rossi, C., Villada, M., Viotti, R., & Baratta, G. B. 1997, in UV Spectroscopy Beyond the IUE Final Archive (ESA-SP 413; Noordwijk: ESA), 353
Saito, M., Sato, H., Saijo, K., & Hayasaka, T. 1980, PASJ, 32, 163
Schmidt-Kaler, T. H. 1982, Physical Parameters of Stars, Landolt-Bornstein New Series, Vol. 2b, Astronomy and Astrophysics, Stars and Star Clusters, ed. K. Schaifers & H. H. Voigt (New York: Springer)
Stalio, R., & Selvelli, P. L. 1981, in The Universe at Ultraviolet Wavelengths: The First Two Years of *IUE*, ed. R. Chapman (NASA CP-2171), 201
Stencel, R. E., Potter, D. E., & Bauer, W. H. 1993, PASP, 105, 45
van de Kamp, P. 1977, AJ, 82, 750
van der Hucht, K. A., Bernat, A. P., & Kondo, Y. 1980, A&A, 82, 14
Wright, K. O. 1970, Vistas Astron., 12, 147
———. 1977, JRASC, 71, 152